

Synthesis, optical, and structural properties of bisphenol-bridged aromatic cyclic phosphazenes*

Bünyemin ÇOŞUT[†], Burcu TOPALOĞLU AKSOY[†], Süreyya Oğuz TUMAY[†],
Ahmet ŞENOCAK[†], Serkan YEŞİLOT^{**†}
Department of Chemistry, Faculty of Science, Gebze Technical University, Gebze, Kocaeli, Turkey

Received: 29.07.2019

Accepted/Published Online: 12.10.2019

Final Version: 11.02.2020

Abstract: Phenoxy- and naphthoxy-substituted bisphenol-bridged cyclic phosphazenes were synthesized in 2 steps and their thermal, photophysical, and electrochemical properties were investigated. The structures of the cyclic phosphazene compounds were determined by ESI-MS mass spectrometry and ¹H, ¹³C, and ³¹P NMR spectroscopies. The photophysical studies of phenoxy- and naphthoxy-substituted bridged cyclophosphazenes were investigated by means of absorption and fluorescence spectroscopies in different solvents. Thermal and electrochemical properties of the target compounds were also studied. Furthermore, the excimer emissions through intramolecular interactions in solution and in solid state were investigated by fluorescence spectroscopy and the theoretical calculations were performed in detail using DFT.

Key words: Cyclotriphosphazene, cyclic voltammetry, fluorescence, DFT, bisphenol A

1. Introduction

In recent years, there has been great interest in the development of new fluorescent materials for many applications, such as light-emitting devices [1], biomedical studies, [2], molecular sensors [3], and solar energy [4]. It is well known that several aromatic hydrocarbons (e.g., benzene, naphthalene, and anthracene) for preparing fluorescent materials are used as themselves or starting materials for new π -conjugated materials [5–7]. In general, they are prepared as small molecules [6,7], dimers [8], or oligomers/polymers [9,10], and for extending π -electron systems. There are many examples of their utility as fluorescent materials in the scientific literature [11]. One reason for further research on aromatic hydrocarbons is that they have high stability and quantum efficiency, leading to the development of fluorescence molecules. Hence, there remains great interest in the design and synthesis of new fluorescence materials using some aromatic hydrocarbons, such as benzene and naphthalene, which were selected herein as new materials.

Cyclic phosphazenes are an important inorganic group of compounds that can be easily substituted using nucleophilic compounds such as phenols, alcohols, and amines via halogen atoms, which are bound to phosphorus atoms [12–15]. They are also important precursors for specialty polymers [16,17]. Due to the chemical and thermal stability of the cyclic phosphazene skeleton, they have various applications, such as biomedical materials [18], flame retardants [19], liquid crystals [20], elastomers [21], or lubricants [22]. Furthermore, cyclophosphazenes have been placed in hybrid polymer electrolytes for lithium ion batteries [21–23]. Aminocyclotriphosphazenes and ferrocenylphosphazenes are 2 of the varying derivatives of phosphazenes. Aminocyclotriphosphazenes have

*Dedicated to supervisor Prof. Dr. Adem Kılıç on his retirement.

**Correspondence: yesil@gtu.edu.tr

shown great antimicrobial activity against bacteria and fungi [21] and ferrocenylphosphazenes have exhibited cytotoxic activity against cancer cells [14,21]. Therefore, new heterocyclic cyclophosphazene structural types have gained attention in both academic and industrial communities [24]. Additionally, cyclic phosphazenes are optically inert in the UV-Vis region; hence, photophysical properties can be adjusted by substituted groups on the phosphorus atoms [13,25–27]. In this manner, cyclic phosphazene- or polyphosphazene-based fluorescent compounds have been prepared for the development of luminescent materials [25,28–30]. Cyclic phosphazenes can vary according to reaction with mono-, bi-, and polydentate reagents. Reaction with difunctional ligands results in spiro-, dispiro-, trispiro-, ansa-, spiro ansa-, or intermolecular products [15,16,21,31].

The precursors $N_3P_3Cl_6$ (trimer) and $N_4P_4Cl_8$ (tetramer) are the most commonly known cyclic phosphazenes and are commercially available. Moreover, owing to optical inertness in the UV-Vis region, they are excellent platforms for the preparation of fluorescent materials for numerous applications, such as fluorescent sensors [32], light-emitting devices [29], electrochromic materials [25], and coordination polymers [33].

In this study, the molecular design, synthesis, and characterization of phenoxy- and naphthoxy-substituted bridged cyclic phosphazenes (Figure 1) are presented, which were obtained by nucleophilic substitution reactions of bisphenol A and cyclic phosphazenes 1–4 at ~80% yields, and their thermal, optical, electrochemical, and structural properties were investigated.

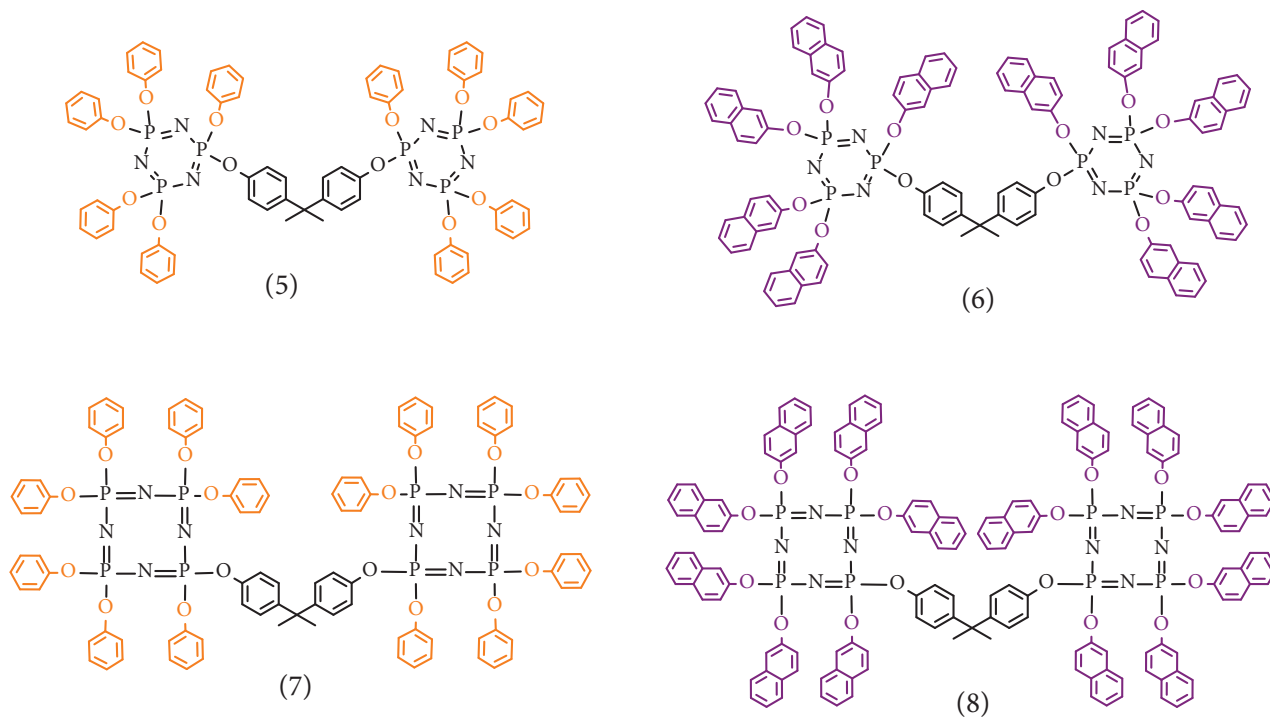


Figure 1. Molecular structures of 5–8.

2. Materials and methods

All reagents were used without further purification and purchased from Sigma-Aldrich (St. Louis, MO, USA), and all solvents were obtained from Merck (Darmstadt, Germany). Reactions were monitored by TLC using Merck TLC silica gel 60 F254. Silica gel column chromatography was used over Merck silica gel 60 (particle size: 0.040–0.063 mm, 230–400 mesh ASTM). 1H , ^{13}C , and ^{31}P NMR spectra were obtained for all of the

compounds in CDCl_3 on a Varian INOVA 500 MHz spectrometer (West Sussex, UK) using TMS as an internal reference for the ^1H and ^{13}C NMR measurements. Thermal properties of the compounds were recorded with a Mettler Toledo TGA/SDTA 851 thermogravimetric analysis (TGA) instrument (Columbus, OH, USA) at a heating rate of $10\text{ }^\circ\text{C}/\text{min}$ under nitrogen. Electronic absorption spectra in the UV-Vis region were measured with a Shimadzu 2101 UV-Vis spectrophotometer (Tokyo, Japan). Fluorescence excitation and emission spectra were obtained on a Varian Eclipse spectrofluorometer (Melbourne, Australia), using 1-cm path-length cuvettes at room temperature. The fluorescence lifetimes were obtained using a Horiba Jobin-Yvon-SPEX Fluorolog 3-2iHR instrument with a Fluoro Hub-B single-photon counting controller (Kyoto, Japan) at an excitation wavelength of 310 nm for compounds **5–8**. Signal acquisition was performed using a TCSPC module.

2.1. Parameters for fluorescence quantum yields

To determine the fluorescence quantum yields (Φ_F) for the target compounds (**5–8**), the comparative calculation method was used [34].

$$\Phi_F = \Phi_{F_{std}} \frac{F \cdot A_{std} \cdot n^2}{F_{std} \cdot A \cdot n_{std}^2} \quad (1)$$

In this equation, F and F_{std} represent the total area below the fluorescence emission spectra of compounds **5–8** and the standard. A and A_{std} are the absorbance of compounds **5–8** and the standard at the excitation wavelength. To calculate the fluorescence quantum yield, refractive indices (n) of the solvents were used due to the dissolution of compounds **5–8** and the standard in different solvents. As one of the most widely used standards in the literature, quinine sulfate ($\Phi_F = 0.54$), which was dissolved in $0.1\text{ M H}_2\text{SO}_4$, was used to calculate the fluorescence quantum yields of compounds **5–8** [35]. The final concentrations of compounds **5–8** were fixed at the same value as the quinine sulfate at the excitation wavelength. Fluorescence lifetimes of compounds **5–8** were directly measured and calculated with monoexponential calculations.

2.2. Synthesis

Compounds **1–4** were synthesized and purified according to literature procedures [5,36–39], respectively.

2.2.1. Synthesis of compound **5**

In a 100-mL 3-necked reaction flask, bisphenol A (0.06 g, 0.3 mmol) and Cs_2CO_3 (0.3 g, 0.6 mmol) were added to compound **1** (0.855 g, 0.6 mmol), dissolved with 25 mL of dry THF. The mixture was stirred under reflux for 72 h and the progress of the reaction was monitored by TLC. The reaction mixture was separated from its salts by filtration through a G4 filter. The solvent of the filtrate (THF) was removed by means of a rotary evaporator. The resulting oily product was purified with column chromatography using THF and n-hexane (1:1) as the mobile phase. Yield: 0.34 g (80%). IR (ATR, room temp.): 1172 cm^{-1} (P=N); 943 cm^{-1} (P-O). MALDI TOF (m/z) calc. 1426.30, found: 1427.55 [M^+]. ^1H NMR (CDCl_3) δ = 7.85–6.53 (m, 58H, ArCH), 3.77 (br, 6H, CH_3); ^{13}C NMR (CDCl_3) δ = 152.05 (ArC), 147.34 (ArC), 146.85 (ArC), 135.90 (ArC), 130.01 (ArCH), 124.07 (ArC), 118.4 (ArCH), 78.5 (ArCH), 68.6 (ArCH $_3$), ^{31}P NMR (toluene- d_8) δ : 9.83 (br, s, 3P).

2.2.2. Synthesis of compound **6**

In a 100-mL 3-necked reaction flask, bisphenol A (0.06 g, 0.3 mmol) and Cs_2CO_3 (0.3 g, 0.6 mmol) were added to compound **2** (1.15 g, 0.6 mmol), dissolved with 25 mL of dry THF. The mixture was stirred under reflux

for 72 h and the progress of the reaction was monitored by TLC. The reaction mixture was separated from its salts by filtration through a G4 filter. The solvent of the filtrate (THF) was removed by means of a rotary evaporator. The resulting oily product was purified with column chromatography using THF and n-hexane (1:1) as the mobile phase. Yield: 0.47 g (81%). IR (ATR, room temp.): 1190 cm^{-1} (P=N); 946 cm^{-1} (P-O). MALDI TOF (m/z) calc. 1926.46, found: 1928.55 $[\text{M}^+]$. ^1H NMR (CDCl_3) d = 7.74–6.88 (m, 58H, ArCH), 3.80 (br, 6H, CH_3); ^{13}C NMR (CDCl_3) d = 151.85 (ArC), 148.54 (ArC), 147.05 (ArC), 136.15 (ArC), 129.6 (ArCH), 125.57 (ArC), 117.9 (ArCH), 77.5 (ArCH), 68.3 (ArCH₃), ^{31}P NMR (toluene-d8) d = 10.63 [m, 4P, >P(OPh)₂, B₂], 10.02 [m, 2P >P(OPh)(OPhO), A]; $^2\text{JP}, \text{P} = 88.86$ Hz.

2.2.3. Synthesis of compound 7

In a 100-mL 3-necked reaction flask, bisphenol A (0.06 g, 0.3 mmol) and Cs_2CO_3 (0.3 g, 0.6 mmol) were added to compound **3** (1.13 g, 0.6 mmol), dissolved with 25 mL of dry THF. The mixture was stirred under reflux for 72 h and the progress of the reaction was monitored by TLC. The reaction mixture was separated from its salts by filtration through a G4 filter. The solvent of the filtrate (THF) was removed by means of a rotary evaporator. The resulting oily product was purified with column chromatography using THF and n-hexane (1:1) as the mobile phase. Yield: 0.5 g (80%). IR (ATR, room temp.): 1187 cm^{-1} (P=N); 945 cm^{-1} (P-O). MALDI TOF (m/z) calc. 1888.39, found: 1890.82 $[\text{M}^+]$. ^{31}P NMR (toluene-d8) d: 11.28 (br, s, 4P). ^1H NMR (CDCl_3) d: 7.29–6.88 (m, 78H, ArCH), 5.07 (br s, 6H, CH_3). ^{13}C NMR (CDCl_3) d: 151.63 (ArC), 149.51 (ArCH), 146.64 (ArC), 136.07 (ArC), 129.43 (ArCH), 127.72 (ArCH), 125.81 (ArCH), 124.61 (ArCH), 121.27 (ArCH), 120.56 (ArCH), 68.21 (ArCH₃).

2.2.4. Synthesis of compound 8

In a 100-mL 3-necked reaction flask, bisphenol A (0.06 g, 0.3 mmol) and Cs_2CO_3 (0.3 g, 0.6 mmol) were added to compound **4** (1.55 g, 0.6 mmol), dissolved with 25 mL of dry THF. The mixture was stirred under reflux for 72 h and the progress of the reaction was monitored by TLC. The reaction mixture was separated from its salts by filtration through a G4 filter. The solvent of the filtrate (THF) was removed by means of a rotary evaporator. The resulting oily product was purified with column chromatography using THF and n-hexane (1:1) as the mobile phase. Yield: 0.65 g (80%). IR (ATR, room temp.): 1165 cm^{-1} (P=N); 950 cm^{-1} (P-O). MALDI TOF (m/z) calc. 2588.61, found: 2590.92 $[\text{M}^+]$. ^1H NMR (CDCl_3) d: 7.71–6.65 (m, 86H, ArCH), 5.08 (br s, 6H, CH_3). ^{13}C NMR (CDCl_3) d: 151.82 (ArC), 149.27 (ArCH), 146.7 (ArC), 136.1 (ArC), 134.06 (ArC), 131.01 (ArC), 129.44 (ArC), 127.85 (ArCH), 126.52 (ArCH), 125.81 (ArCH), 125.33 (ArCH), 120.40 (ArCH), 117.74 (ArCH), 68.26 (ArCH₃).

3. Results and discussion

3.1. Synthesis, characterization, and thermal analysis

The synthetic pathways to compounds **1–8** presented in this work are shown in Figure 2. Compound **1** was synthesized by the reaction of phenol with hexachlorocyclotriphosphazene (trimer) in the presence of Cs_2CO_3 in THF. Compound **2** was obtained by the reaction of 2-naphthol with trimer in the presence of Cs_2CO_3 as the base in THF. For the synthesis of compounds **4** and **5**, octachlorocyclotetraphosphazene (tetramer) was reacted with phenol and 2-naphthol, respectively. For the synthesis of bisphenol-bridged cyclophosphazene compounds, nucleophilic displacement reactions between the bisphenol and phenol and 2-naphthol decorated trimer and

tetramer were performed under an argon atmosphere. The obtained phenol and 2-naphthol decorated cyclic phosphazene compounds were reacted with bisphenol at a 2:1 ratio in the presence of cesium carbonate in THF. The products were purified by preparative TLC on silica gel using hexane and THF (1:1) as the mobile phase.

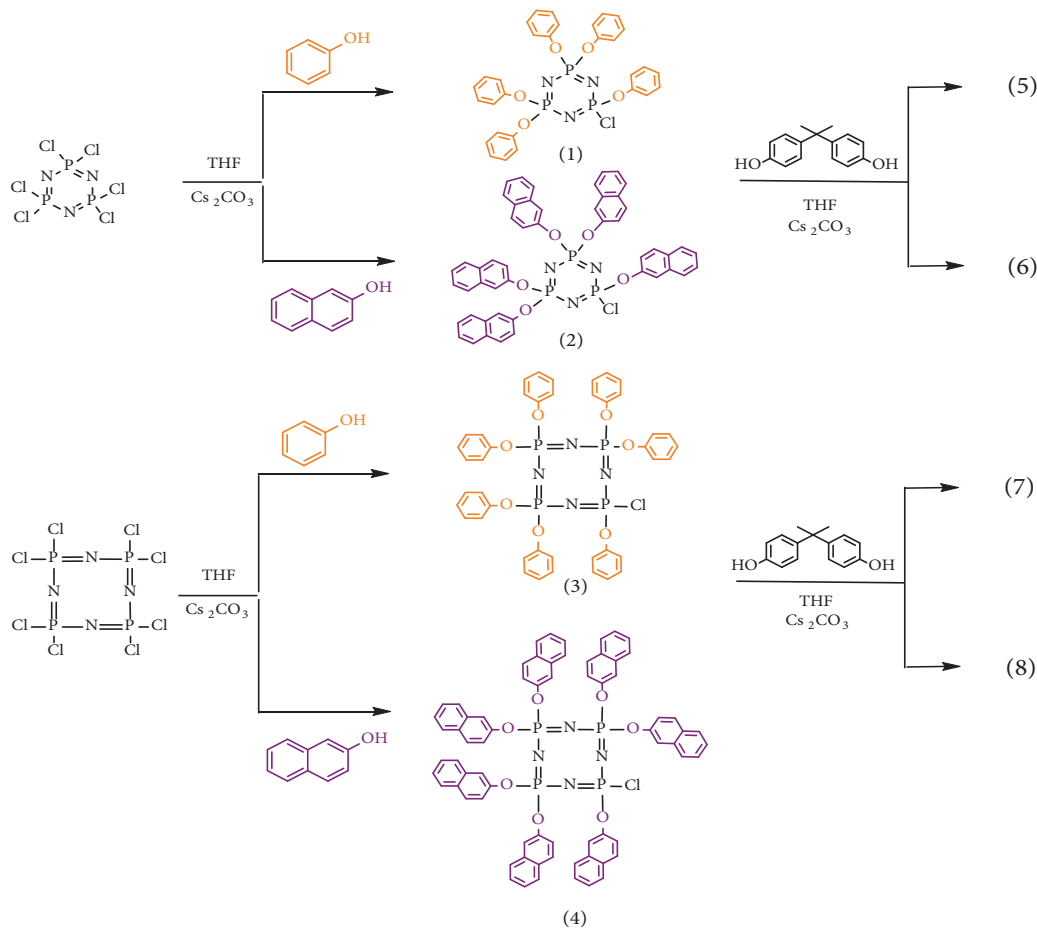


Figure 2. Synthetic route to compounds 1–8.

The synthesized compounds were characterized by ^1H , ^{13}C , and ^{31}P NMR, mass and infrared spectrometry, and thermal analysis. All of the results were consistent with the predicted structures. The results are summarized in the Section 2 and the ^{31}P NMR and infrared spectra, thermal analysis, and mass results are given in the Supplemental information. In particular, the newly synthesized compounds were subjected to ^{31}P NMR spectroscopy analysis in order to confirm the targeted structures. For instance, the obtained ^{31}P NMR spectra (proton-decoupled) of compounds **5** and **7** showed A_3 and A_4 spin systems with the same chemical environment, respectively (Figures S1 and S2), which confirmed the suggested structures. It should be noted that the phenoxy units of the bisphenol, which were introduced into the bridgehead, had the same chemical environment as the other phenoxy-substituted phosphorus atoms. ^{31}P NMR spectra of compounds **6** and **8** were somewhat more complex, due to having different chemical environments than the phosphorus atoms. The ^{31}P NMR spectrum of compound **6** showed a typical AB_2 spin system and gave rise to very close compound **8**, and the calculated chemical shifts and coupling constants were at 10.63 ppm for $>\text{P}(\text{OPh})$, 10.02 ppm for

$>P(OPh)(OPhO)$, and 88.86 Hz (${}^2J_{P,P}$), respectively (Figures S3 and S4). As can be seen in Figure S4, the ${}^{31}P$ NMR spectrum of compound **8** was more complex and might be an AB_2C spin system; however, it was not possible to assign its coupling constants. In addition, the mass spectra of compounds **5–8** were consistent with the predicted structures (Figures S5–S8). According to the obtained FTIR spectra of the compounds, the P=N and P-O stretches were shown at 1172 cm^{-1} and 943 cm^{-1} for compound **5**, 1190 cm^{-1} and 946 cm^{-1} for compound **6**, 1187 cm^{-1} and 945 cm^{-1} for compound **7**, and 1165 cm^{-1} and 950 cm^{-1} for compound **8**, respectively (Figure S9).

TGA methods were used to investigate the thermal stability of all of the cyclophosphazene compounds (Figure S10). In the TGA analysis measurements of the compounds under nitrogen (N_2) gas with heating at 10 $^{\circ}C/min$ up to 700 $^{\circ}C$, the temperatures at which 5% decomposition for compounds **5–8** occurred were 465, 475, 460, and 477 $^{\circ}C$, respectively.

3.2. Optical and electrochemical properties

Photophysical properties of the phenoxy- and naphthoxy-substituted cyclic trimeric and tetrameric phosphazene compounds (**5** and **6**, and **7** and **8**) were evaluated with UV-Vis absorption and fluorescence emission experiments. UV-Vis absorptions of the phenoxy-substituted cyclic trimeric and tetrameric phosphazene compounds (**5** and **7**) and naphthoxy-substituted cyclic trimeric and tetrameric phosphazene compounds (**6** and **8**) were measured in different solvents. As can be seen in Figure 3, compounds **5** and **7** demonstrated absorption maxima at 263 nm with an absorption band between ≈ 250 and 70 nm, whereas compounds **6** and **8** demonstrated absorption maxima at 272 nm with an absorption band between ≈ 260 and 288 nm. The observed absorption behaviors of compounds **5–8** can be attributed to the $\pi-\pi^*$ transitions of the phenoxy and naphthoxy groups, which appended on the cyclic trimeric and tetrameric phosphazenes [32,40–42]. This means that compounds **5–8** demonstrated similar absorption behaviors with phenoxy and naphthoxy, and this is a well-known phenomenon for phosphazene compounds, which are photophysically inert in the UV-Vis region [29,30]. In addition, these results showed that the phenoxy and naphthoxy groups on the cyclic trimeric and tetrameric phosphazenes had no effective ground state interaction.

After evaluation of the UV-Vis absorptions of compounds **5–8**, their fluorescence emission behaviors were examined under the same conditions as in the absorption studies. Fluorescence emission spectra of the target compounds are given in Figure 4, in which compounds **5** and **7** were excited at 260 nm and compounds **6** and **8** were excited at 290 nm. According to Figure 4, normalized fluorescence spectra of 5×10^{-5} M for compounds **5** and **7** demonstrated classic monomer phenolic emission at ~ 290 nm [43], whereas under the same conditions, compounds **6** and **8** demonstrated excimer emission, which arose from the $\pi-\pi$ stacking interaction between the naphthol units on the cyclic trimeric and tetrameric phosphazenes at ~ 390 nm. These red-shifted emission wavelengths of **6** and **8** increased up to 54 nm when compared to monomer naphthol emissions [44].

This bathochromic shift of compounds **6** and **8** was very similar to intermolecular excimer emission, and it is well known that intermolecular excimer formation is a concentration-dependent phenomenon and does not occur in dilute media [45]. In addition, the dissolution medium of compounds can affect monomer and excimer formation [46,47]. As can be seen in Figure 4, the monomeric phenol emissions of 5×10^{-5} M in compounds **5** and **7** and excimer emissions of 5×10^{-5} M in compounds **6** and **8** were not affected by the solvent system. According to the obtained results, the molar absorptivities of compounds **5–8** in different solvents were calculated and are given in Table 1.

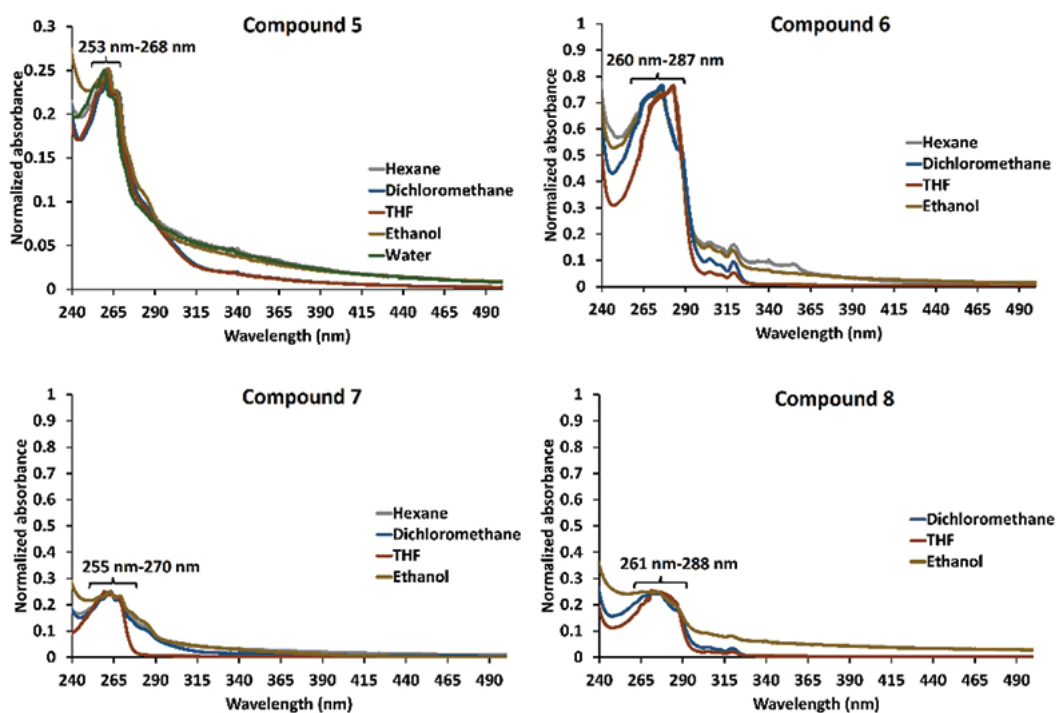


Figure 3. Normalized UV-Vis absorption spectra of compounds 5, 6, 7, and 8 in different solvents.

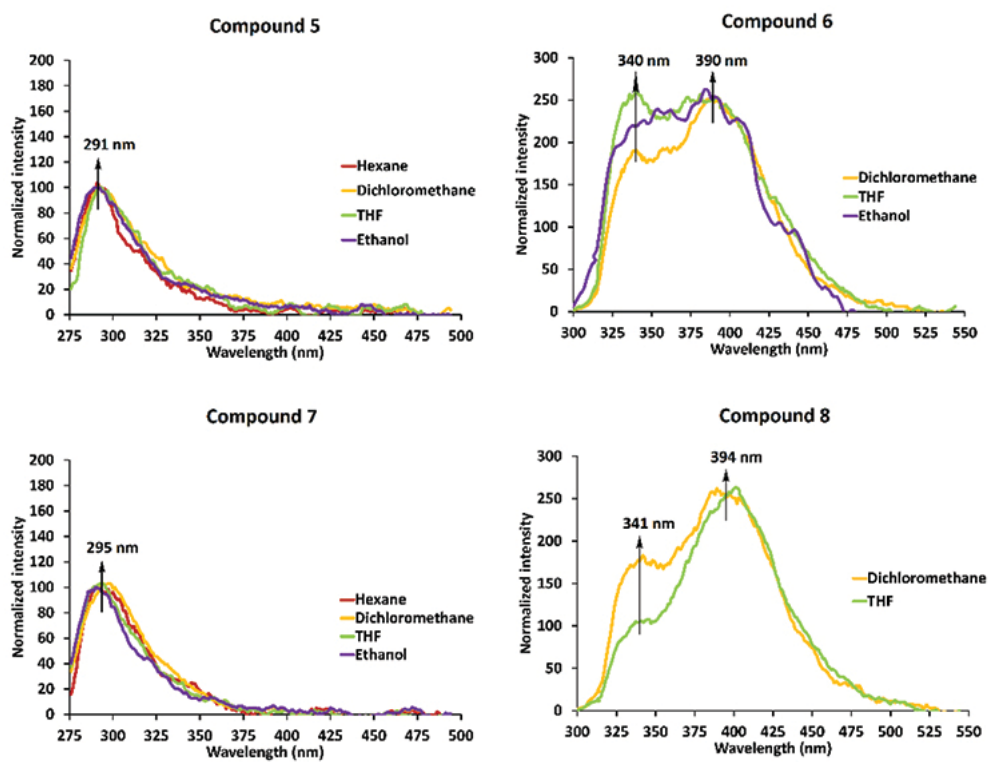


Figure 4. Normalized fluorescence emission spectra of compounds 5, 6, 7, and 8 in different solvents ($\lambda_{exc.}$: 260 nm for 5 and 7, and $\lambda_{exc.}$: 290 nm for 6 and 8).

Table 1. Molar absorptivity of compounds **5–8**.

ε (L mol ⁻¹ cm ⁻¹)	Hexane	Dichloromethane	THF	Ethanol	Water
5	3700	9600	8000	5000	2500
6	5300	54,000	55,000	10,000	1400
7	5400	11,000	9600	4200	1500
8	790	35,000	32,000	3400	1600

To evaluate the effect of concentration on the photophysical behaviors of compounds **5–8**, the UV-Vis absorption and fluorescence emission spectra were examined at different concentrations in various solvents, such as hexane, dichloromethane (DCM), THF, ethanol, and water (Figures S11–S18). As can be seen in Figures S11–S18, compounds **5–8** were slightly soluble in hexane and water. In addition, the UV-Vis electronic absorption and fluorescence emission signals of compounds **5–8** decreased proportional to the concentration, and the monomeric phenol emissions of compounds **5** and **7** and excimer emissions of compounds **6** and **8** were consistent in diluted or concentrated media. These results showed that there was no intermolecular self-quenching, which was observed at high concentrations in compounds **5–8** [48]. Moreover, the excimer emission of compounds **6** and **8** was observed in a dilute concentration, which indicated that the intramolecular π - π stacking interaction between the naphthol units on the cyclic trimeric and tetrameric phosphazenes was the source of the excimer emission [32,46,47].

An important property of fluorescence dyes is a large Stokes shift, which reduces self-absorption, and this was calculated for compounds **5–8** in CH₂Cl₂ and is given in Figure 5 [49]. According to Figure 5, the Stokes shifts of compounds **5** and **7** were calculated as 28 nm and 30 nm, respectively, whereas the Stokes shifts of compounds **6** and **8** were determined as 118 nm for both compounds. This large Stokes shift of compounds **6** and **8** can be attributed to intramolecular π - π stacking interactions between the naphthol units on the cyclic trimeric and tetrameric phosphazenes. The fluorescence lifetimes (τ_F) of compounds **5–8** were calculated with monoexponential calculation as 0.131 ± 0.007, 13.542 ± 0.059, 0.147 ± 0.008, and 17.143 ± 0.045 ns, respectively (Figure 6). In addition, the fluorescence quantum yields (Φ_f) of compounds **5–8** were calculated as 0.07, 0.29, 0.075, and 0.31, respectively, when quinine sulfate ($\Phi_F = 0.54$) was used as the standard. The obtained results for the τ_F and Φ_f are given in Table 2.

Table 2. Fluorescence quantum yields (Q_F) and lifetimes of compounds **5–8**.

	5	6	7	8
Q_F (DCM)	0.070	0.280	0.075	0.310
τ (ns)	0.131 ± 0.007	13.542 ± 0.059	0.147 ± 0.008	17.143 ± 0.045

The cyclic voltammetry (CV) measurements were performed with the CH Instruments 440B electrochemical system (Bee Cave, TX, USA) (Figure 7). A glassy carbon electrode, Pt wire, and saturated calomel electrode served as the working, counter, and reference electrodes. Electrochemical grade tetrabutylammonium hexafluorophosphate (TBAPF₆) in extra pure DCM was used as the supporting electrolyte in CV at a concentration of 0.10 mol dm⁻³. High purity N₂ was used for deoxygenation of the solution for 10 min prior to each run and maintained in a nitrogen blanket [50,51]. HOMO-LUMO levels and band gap values provide further information on the potential use of a new molecule for many applications, such as dye-sensitized and organic

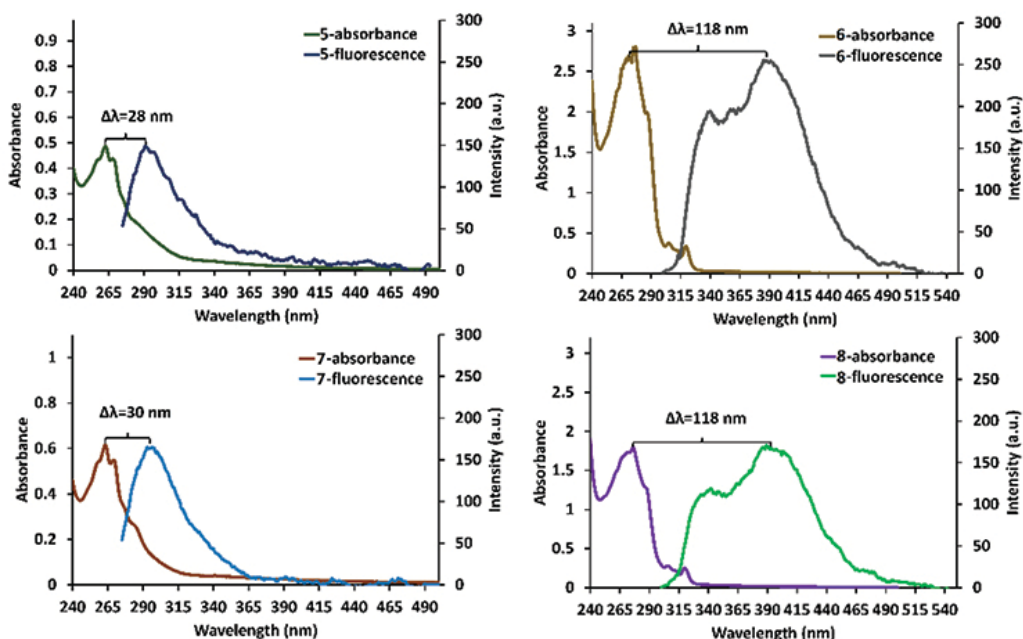


Figure 5. Stoke shifts of compounds **5**, **6**, **7**, and **8** in DCM ($\lambda_{exc.}$: 260 nm for **5** and **7**, and $\lambda_{exc.}$: 290 nm for **6** and **8**).

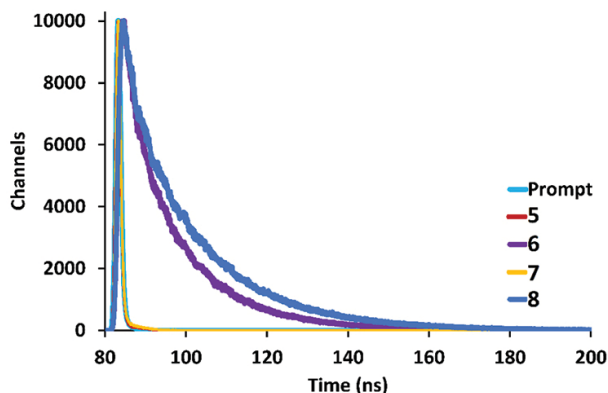


Figure 6. Fluorescence lifetime decays of compounds **5**, **6**, **7**, and **8**.

solar cells. HOMO-LUMO energy levels were determined by 3 different methods including UV-Vis absorption onset (λ_{onset}) and CV and DFT calculations. In the current study, the 3 methods used to estimate these values are summarized in Table 3.

HOMO and LUMO energy levels of compounds **5–8** were calculated using the first oxidation and reduction values from CV. The corresponding HOMO energy levels of compounds **5–8** were calculated as -5.64 , -5.53 , -5.63 , and -5.53 eV, respectively, using the equation $E_{HOMO} = -[(E_{ox} - E_{1/2(ferrocene)}) + 4.8]$. The LUMO energy levels of these compounds were determined as -1.44 , -1.78 , -1.50 , and -1.78 eV, respectively, using the UV-Vis spectra of these compounds. Band gap values of the compounds were determined as 3.12, 2.99, 3.05, and 2.99, respectively, from the electrochemical measurements. Moreover, band gaps were calculated from the UV-Vis absorption band onset (λ_{onset}) by the equation $E_g(\text{eV}) = 1240/\lambda_{onset}(\text{nm})$ and determined as 4.20, 3.75, 4.13, and 3.75 for compounds **5–8**, respectively. HOMO and LUMO orbitals and energy gap levels were

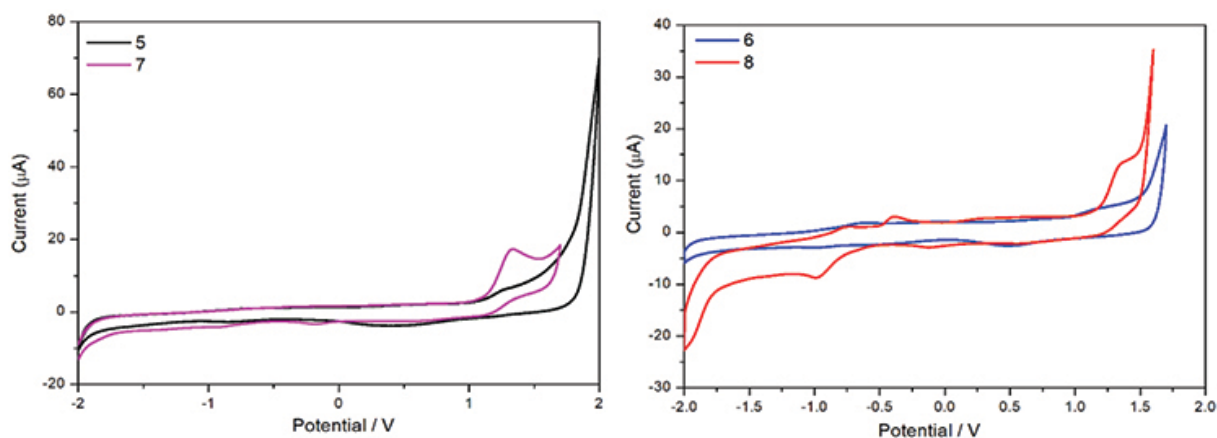


Figure 7. Cyclic voltammogram of compounds 5, 6, 7, and 8.

Table 3. HOMO and LUMO energy level values determined from the experimental CV, theoretical calculations, and band gap energy values.

		5	6	7	8
E_{ox}		1.24	1.13	1.23	1.32
E_{HOMO}	CV	-5.64	-5.53	-5.63	-5.53
	DFT	-6.10	-5.55	-5.96	-5.54
E_{LUMO}	UV/CV*	-1.44	-1.78	-1.50	-1.78
	DFT	-0.26	-1.13	-0.20	-1.07
E_g (cyclic)		3.12	2.99	3.05	2.99
E_g (optical)		4.20	3.75	4.13	3.75
E_g (DFT)		5.84	4.42	5.76	4.47

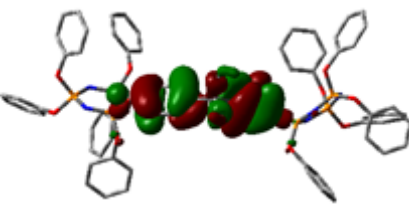
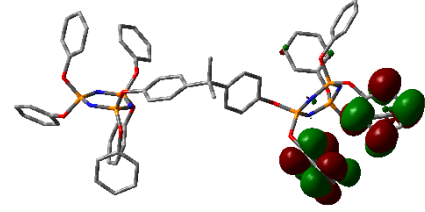
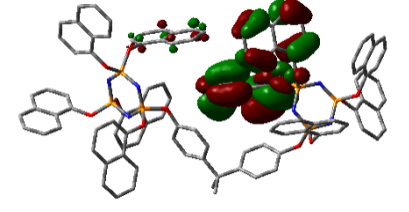
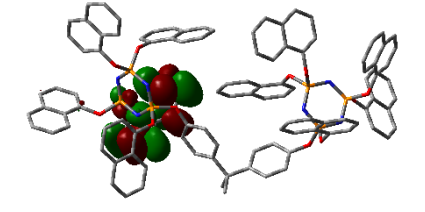
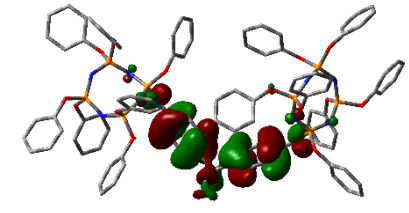
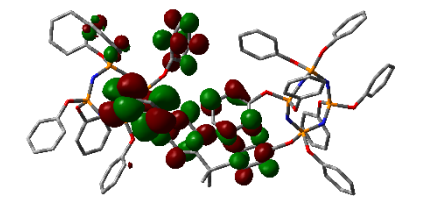
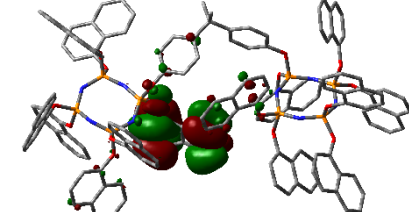
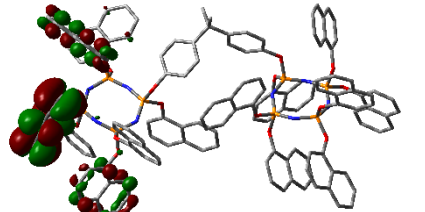
*The band gap (E_g) was calculated from the onset absorption edge in the UV-Vis spectra of compounds 5–8 and was found as 4.20, 3.75, 4.13, and 3.75 eV, respectively, and then the LUMO could be estimated as -1.44, -1.78, -1.50, and -1.78 eV, respectively.

also calculated by performing single-point time-dependent DFT (TD-DFT) calculations using the B3LYP/6-31G (d, p) levels (Table 4). HOMO-LUMO energies of compounds 5–8 are tabulated in Table 3 and the band gap values from the DFT calculation were determined as 5.84, 4.42, 5.76, and 4.47, respectively. These findings showed that these molecules were located at high energy levels and the large band gaps make these molecules potentially useful in electronics, light-emitting diodes, and solar cells.

3.3. Computational results

The Gaussian 09 package was used for all theoretical computations, which were performed via DFT to obtain more information about the optimized structures of the new compounds and their intramolecular interactions among the phenol and naphthol groups [52]. Geometry optimization studies were performed by B3LYP with a basis set of 6-31G (d, p) and the nearest values to the crystal structure could be obtained with this method [53]. The optimized geometries of compounds 5–8 are illustrated in Figure 8. Although phenoxy-substituted phosphazene molecules 5 and 7 did not exhibit any intramolecular interactions, naphthol-containing phosphazene compounds 6 and 8 exhibited intramolecular noncovalent interactions. The distances of the

Table 4. HOMO-LUMO orbitals of compounds **5**, **6**, **7**, and **8**.

Compound	HOMO	LUMO
5		
6		
7		
8		

phenoxy and naphthoxy groups for compounds **6** and **8** are illustrated in Figure 9. The selected intramolecular naphthoxy groups were in the range of 3.79 to 3.98 Å, which is within the accepted range for π - π interaction of less than 4.0 Å [46]. According to the results of the DFT calculations, while excimer emissions occurred within the molecules in compounds **6** and **8**, monomer emissions occurred in compounds **5** and **7**, but they were not within the molecules, and the theoretical results were in perfect harmony with the fluorescence results.

4. Conclusions

To summarize, we presented the design, synthesis, and characterization of phenoxy- and naphthoxy-substituted bisphenol-bridged cyclic phosphazenes (**5–8**). Standard spectroscopic techniques, such as ESI-MS, ^1H , ^{13}C , and ^{31}P were used for the characterization of compounds **5–8**. The thermal, optical, electrochemical, and structural properties of the target bridged cyclic phosphazenes (**5–8**) were investigated by TGA, UV-Vis, and fluorescence spectroscopies and CV and DFT calculations, respectively. According to the UV-Vis and fluorescence measurements, the naphthoxy-substituted bisphenol-bridged cyclic phosphazenes (**6** and **8**) showed excimer emissions while their phenoxy derivatives (**5** and **7**) demonstrated only monomer emissions at 290 nm,

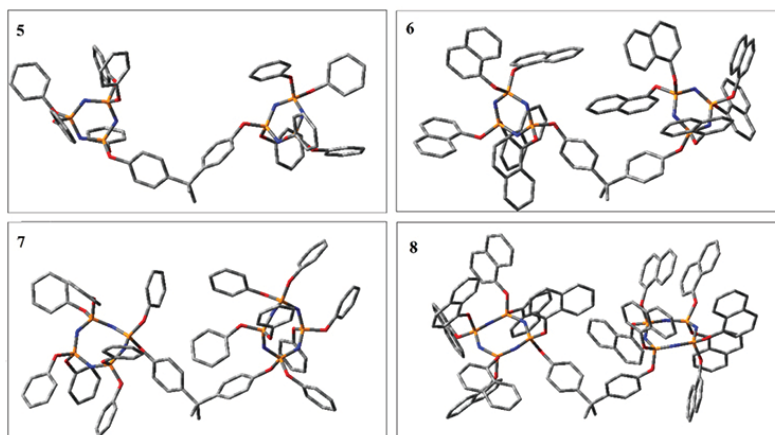


Figure 8. Optimized geometries of compounds **5**, **6**, **7**, and **8** using B3LYP/6-31G (d, p) levels.

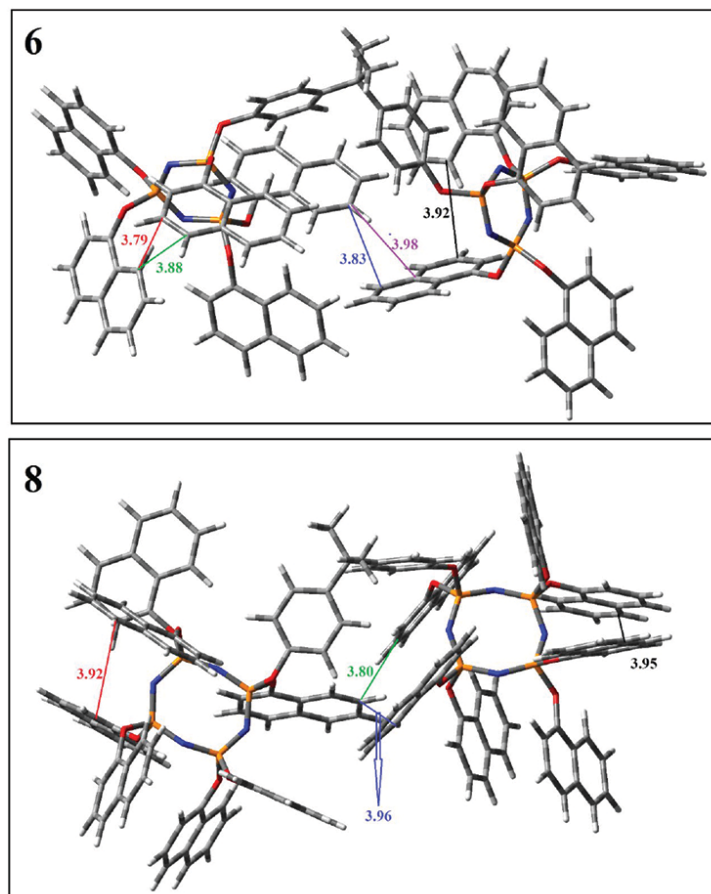


Figure 9. Selected intramolecular π - π interactions in the structures of compounds **6** and **8**.

which was confirmed by theoretical calculations. In addition, the HOMO and LUMO orbitals and energy gap levels were calculated and confirmed by electrochemical measurements, UV-Vis absorption band onset, and single-point (TD-DFT) calculations. According to all of the investigations, compounds **5–8** are potential candidates for important industrial applications, such as light-emitting diodes, solar cells, and flame retardants.

References

1. Astruc D, Boisselier E, Ornelas C. Dendrimers designed for functions: from physical, photophysical, and supramolecular properties to applications in sensing, catalysis, molecular electronics, photonics, and nanomedicine. *Chemical Reviews* 2009; 110: 1857-1959. doi: 10.1021/cr900327d
2. Singler RE, Willingham RA, Noel C, Friedrich C, Bosio L et al. Thermotropic liquid crystalline poly (organophosphazene). *Macromolecules* 1991; 24: 510-516. doi: 10.1021/ma00002a026
3. Wu D, Sedgwick AC, Gunnlaugsson T, Akkaya EU, Yoon J et al. Fluorescent chemosensors: the past, present and future. *Chemical Society Reviews* 2017; 6: 7105-7123. doi: 10.1039/C7CS00240H
4. Giordano F, Roma G, Liberatore M, Miruzzo V, Conte V. Smart materials and concepts for photovoltaics: dye sensitized solar cells. *Smart Materials for Energy, Communications and Security* 2008; 97-126. doi: 10.1007/978-1-4020-8796-7_8
5. Çoşut B, Yeşilot S. Synthesis, thermal and photophysical properties of naphthoxycyclotriphosphazeny-substituted dendrimeric cyclic phosphazenes. *Polyhedron* 2012; 35: 101-107. doi: 10.1016/j.poly.2012.01.013
6. Zhang W, Zhao X, Gu W, Cheng T, Wang B et al. A novel naphthalene-based fluorescent probe for highly selective detection of cysteine with a large Stokes shift and its application in bioimaging. *New Journal of Chemistry* 2018; 42: 18109-18116. doi: 10.1039/C8NJ04425B
7. Badekar PS, Kumbhar AA. Anthracene-based fluorescence turn-on chemodosimeter for the recognition of persulfate anion. *New Journal of Chemistry* 2018; 42: 3917-3923. doi: 10.1039/C7NJ03425C
8. Wei AP, Blumenthal DK, Herron JN. Antibody-mediated fluorescence enhancement based on shifting the intramolecular dimer monomer equilibrium of fluorescent dyes. *Analytical Chemistry* 1994; 66: 1500-1506. doi: 10.1021/ac00081a023
9. Dunsing V, Luckner M, Zühlke B, Petazzi RA, Herrmann A et al. Optimal fluorescent protein tags for quantifying protein oligomerization in living cells. *Scientific Reports* 2018; 2018: 1-12. doi: 10.1038/s41598-018-28858-0
10. Smith RC, Tennyson AG, Lim MH, Lippard SJ. Conjugated polymer-based fluorescence turn-on sensor for nitric oxide. *Organic Letters* 2005; 7: 3573-3575. doi: 10.1021/ol0513903
11. Tuncel D. π -Conjugated nanostructured materials: preparation, properties and photonic applications. *Nanoscale Advances* 2019; 1: 19-33. doi: 10.1039/C8NA00108A
12. Allen CW. Regio- and stereochemical control in substitution reactions of cyclophosphazenes. *Chemical Reviews* 1991; 91: 119-135. doi: 10.1021/cr00002a002
13. Özcan E, Tümay SO, Keşan G, Yeşilot S, Çoşut B. The novel anthracene decorated dendrimeric cyclophosphazenes for highly selective sensing of 2,4,6-trinitrotoluene (TNT). *Spectrochimica Acta Part A: Molecular and Biomolecular Spectroscopy* 2019; 220: 117115. doi: 10.1016/j.saa.2019.05.020
14. Keshav K, Singh N, Elias JA. Synthesis and reactions of ethynylferrocene-derived fluoro- and chlorocyclotriphosphazenes. *Inorganic Chemistry* 2010; 49: 5753-5765. doi: 10.1021/ic100703h
15. Kumar D, Singh N, Keshav K, Elias JA. Ring-closing metathesis reactions of terminal alkene-derived cyclic phosphazenes. *Inorganic Chemistry* 2011; 50: 250-260. doi: 10.1021/ic101884s
16. Kumar NS, Swamy Kumara KC. Synthesis and structures of unsymmetrical bis- and tris-cyclotriphosphazenes. *Polyhedron* 2004; 23: 979-985. doi: 10.1016/j.poly.2003.12.024
17. Kumarasswamy S, Vijjulatha M, Muthiah C, Swamy Kumara KC, Engelhardt U. Synthesis, reactivity and structures of spirocyclic products derived from octachlorocyclotetraphosphazene: comparison with spirocyclic cyclotriphosphazenes and linear phosphazenes. *Dalton Transactions* 1999; 891-899. doi: 10.1039/A807373B

18. Ozay H, Ozay O. Synthesis and characterization of drug microspheres containing phosphazene for biomedical applications. *Colloids and Surfaces A: Physicochemical and Engineering Aspects* 2014; 450: 99-105. doi: 10.1016/j.colsurfa.2014.03.022
19. Sun J, Yu Z, Wang X, Wu D. Synthesis and performance of cyclomatrix polyphosphazene derived from trispirocyclotriphosphazene as a halogen-free nonflammable material. *Sustainable Chemistry Engineering* 2014; 2: 231-238. doi: 10.1021/sc400283d
20. He Q, Dai H, Tan X, Cheng X, Liu F et al. Synthesis and characterization of room temperature columnar mesogens of cyclotriphosphazene with Schiff base units. *Journal of Material Chemistry C* 2013; 1: 7148-7154. doi: 10.1039/C3TC31371A
21. Tümer Y, Asmafiliz N, Kılıç Z, Aydın B, Açık L et al. Phosphorus-nitrogen compounds: Part 43. Syntheses, spectroscopic characterizations and antimicrobial activities of *cis*- and *trans*-N/O dispirocyclotriphosphazenes containing ferrocenyl pendant arms. *Journal of Molecular Structure* 2018; 1173: 885-893. doi: 10.1016/j.molstruc.2018.07.050
22. Keller MA, Saba CS. Oxidative stability and degradation mechanism of a cyclotriphosphazene lubricant. *Analytical Chemistry* 1996; 68 (19): 3489-3492. doi: 10.1021/ac960632x
23. Zuo C, Yang M, Wang Z, Jiang K, Li S et al. Cyclophosphazene-based hybrid polymer electrolytes obtained *via* epoxy-amine reaction for high-performance all-solid-state lithium-ion batteries. *Journal of Material Chemistry A* 2019; 7: 18871-18879. doi: 10.1039/C9TA05028K
24. Lawson GT, Rivals F, Tascher M, Jacob C, Bickley JF et al. *cis*-Trihydrogen cyclotriphosphazenes—acidic anions in strongly basic media. *Chemical Communications* 2000; 341-342. doi: 10.1039/A908954C
25. Çetindere S, Tümay SO, Şenocak A, Kılıç A, Durmuş M et al. Novel pyrene-BODIPY dyes based on cyclotriphosphazene scaffolds: synthesis, photophysical and spectroelectrochemical properties. *Inorganica Chimica Acta* 2019; 494: 132-140. doi: 10.1016/j.ica.2019.05.022
26. AlidağıArdıç H, Tümay SO, Şenocak A, Yeşilot S. Pyrene functionalized cyclotriphosphazene-based dyes: synthesis, intramolecular excimer formation, and fluorescence receptor for the detection of nitro-aromatic compounds. *Dyes and Pigments* 2018; 153: 172-181. doi: 10.1016/j.dyepig.2018.02.012
27. Tümay SO, Uslu A, AlidağıArdıç H, Kazan HH, Bayraktar C et al. A systematic series of fluorescence chemosensors with multiple binding sites for Hg(II) based on pyrenyl-functionalized cyclotriphosphazenes and their application in live cell imaging. *New Journal of Chemistry* 2018; 42: 14219-14228. doi: 10.1039/C8NJ02482K
28. Xu J, Toh CL, Ke KL, Li JJ, Cho CM et al. Thermally stable blue-light-emitting hybrid organic – inorganic polymers derived from cyclotriphosphazene. *Macromolecules* 2008; 41: 9624-9636. doi: 10.1021/ma801563s
29. AlidağıArdıç H, Hacıvelioğlu F, Tümay SO, Çosut B, Yeşilot S. Synthesis and spectral properties of fluorene substituted cyclic and polymeric phosphazenes. *Inorganica Chimica Acta* 2017; 457: 95-102. doi: 10.1016/j.ica.2016.12.013
30. Çetindere S, Tümay SO, Kılıç A, Durmuş M, Yeşilot S. Synthesis and physico-chemical properties of cyclotriphosphazene-BODIPY conjugates. *Dyes and Pigments* 2017; 139: 517-523. doi: 10.1016/j.dyepig.2016.12.035
31. Kumar Bhuvan NN, Swamy Kumara KC. Single diastereomers of unsymmetrical tris-spirocyclic cyclotriphosphazenes based on 1,1'-bi-2-naphthol—Synthesis and structures. *Chirality* 2008; 20: 781-789. doi: 10.1002/chir.20528
32. Tümay SO, Yeşilot S. Tripodal synthetic receptors based on cyclotriphosphazene scaffold for highly selective and sensitive spectrofluorimetric determination of iron(III) in water samples. *Journal of Photochemistry & Photobiology A: Chemistry* 2019; 372: 156-167. doi: 10.1016/j.jphotochem.2018.12.012
33. Seçkin T, Sezer S, Köytepe S. Synthesis of phenanthroline-functionalized phosphazene based metallosupramolecular polymers and their stimuli-responsive properties. *Journal of Inorganic Organometallic Polymers and Materials* 2018; 28 (6): 2825-2834. doi: 10.1007/s10904-018-0938-0

34. Fery-Forgues S, Lavabre D. Are fluorescence quantum yields so tricky to measure? A demonstration using familiar stationary products. *Journal of Chemical Education* 1999; 76 (9): 1260-1264. doi: 10.1021/ed076p1260
35. Melhuish WH. Quantum efficiencies of fluorescence of organic substances: effect of solvent and concentration of the fluorescent solute. *Journal of Physical Chemistry* 1961; 65: 229-235. doi: 10.1021/j100820a009
36. Durmuş M, Hacivelioglu F, Kılıç A, Yeşilot S. The synthesis, thermal and photophysical properties of phenoxy-cyclotriphosphazeny- substituted cyclic and polymeric phosphazenes. *Polyhedron* 2009; 28: 2510-2516. doi: 10.1016/j.poly.2009.05.027
37. Çoşut B, Yeşilot S, Durmuş M, Kılıç A, Ahsen V. Synthesis and properties of axially-phenoxy-cyclotriphosphazeny- substituted silicon phthalocyanine. *Polyhedron* 2010; 29: 675-682. doi: 10.1016/j.poly.2009.09.035
38. Okutan E, Çoşut B, Kayıran BS, Durmuş M, Kılıç A. Synthesis of a dendrimeric phenoxy-substituted cyclotetraphosphazene and its non-covalent interactions with multiwalled carbon nanotubes. *Polyhedron* 2014; 67: 344-350. doi: 10.1016/j.poly.2013.09.011
39. Şenkuytu E, Yenilmez Çiftçi G. Structural and chemosensor properties of FDA and FDP derivatives of fluorenylidene bridged cyclotetraphosphazenes. *Polyhedron* 2016; 115: 247-256. doi: 10.1016/j.poly.2016.04.046
40. Ren H, Jia S, Wu Y, Wu S, Zhang T et al. Improved photochemical reactivities of Ag₂O/g-C₃N₄ in phenol degradation under UV and visible light. *Industrial Engineering Chemical Research* 2014; 53: 17645-17653. doi: 10.1021/ie503312x
41. Tchaikovskaya ON, Sokolova IV, Kuznetsova RT, Swetlitchnyi VA, Kopylova TN et al. Fluorescence investigations of phenol phototransformation in aqueous solutions. *Journal of Fluorescence* 2000; 10: 403-408. doi: 10.1023/A:1009486615346
42. Xiao D, Premont-Schwarz M, Nibbering ETJ, Batista VS. Ultrafast vibrational frequency shifts induced by electronic excitations: naphthols in low dielectric media. *Journal of Physical Chemistry A* 2012; 116: 2775-2790. doi: 10.1021/jp208426v
43. Zhao X, Li Y, Wang J, Ouyang Z, Li J et al. Interactive oxidation-reduction reaction for the in situ synthesis of graphene-phenol formaldehyde composites with enhanced properties. *Applied Materials Interface* 2014; 6: 4254-4263. doi: 10.1021/am405983a
44. Parker D, Williams JA. Luminescence behaviour of cadmium, lead, zinc, copper, nickel and lanthanide complexes of octadentate macrocyclic ligands bearing naphthyl chromophores. *Journal of Chemical Society, Perkin Transactions 2* 1995; 7: 1305-1314. doi: 10.1039/P29950001305
45. Kamkaew A, Burgess K. Aza-BODIPY dyes with enhanced hydrophilicity. *Chemical Communications* 2015; 51: 10664-10667. doi: 10.1039/C5CC03649F
46. Yeşilot S, Çoşut B, AlidağıArdıç H, Hacivelioglu F, Özpınar AG et al. Intramolecular excimer formation in hexakis(pyrenyloxy)cyclotriphosphazene: photophysical properties, crystal structure, and theoretical investigation. *Dalton Transactions* 2014; 43: 3428-3433. doi: 10.1039/C3DT52957F
47. Tümay SO, Sarıkaya YS, Yeşilot S. Novel iron(III) selective fluorescent probe based on synergistic effect of pyrene-triazole units on a cyclotriphosphazene scaffold and its utility in real samples. *Journal of Luminescence* 2018; 196: 126-135. doi: 10.1016/j.jlumin.2017.12.019
48. Du Y, Chen M, Zhang Y, Luo F, He C et al. Determination of iron(III) based on the fluorescence quenching of rhodamine B derivative. *Talanta* 2013; 106: 261-265. doi: 10.1016/j.talanta.2012.10.078
49. Gu B, Huang L, Mi N, Yin P, Zhang Y et al. An ESIPT-based fluorescent probe for highly selective and ratiometric detection of mercury(II) in solution and in cells. *Analyst* 2015; 140: 2778-2784. doi: 10.1039/C5AN00273G

50. Şenocak A, Kaya EN, Kadem B, Basova T, Demirbaş E et al. Synthesis and organic solar cell performance of BODIPY and coumarin functionalized SWCNTs or graphene oxide nanomaterials. Dalton Transactions 2018; 47: 9617-9626. doi: 10.1039/C8DT01588K
51. Şenocak A, Köksoy B, Demirbaş E, Durmuş M. Investigation of electrochemical properties and gas adsorption studies of novel sandwich core phthalocyanines. Journal of Physical Organic Chemistry 2018; 32: 1-12. doi: 10.1002/poc.3907
52. Frisch MJ, Trucks GW, Schlegel HB, Scuseria GE, Robb MA et al. Gaussian 09, Revision B.01, 2009. Wallingford, CT, USA: Gaussian; 2009.
53. Becke AD. Density functional thermochemistry. III. The role of exact exchange. Journal of Chemical Physics 1993; 98: 5648-5652. doi: 10.1063/1.464913

Supplemental information

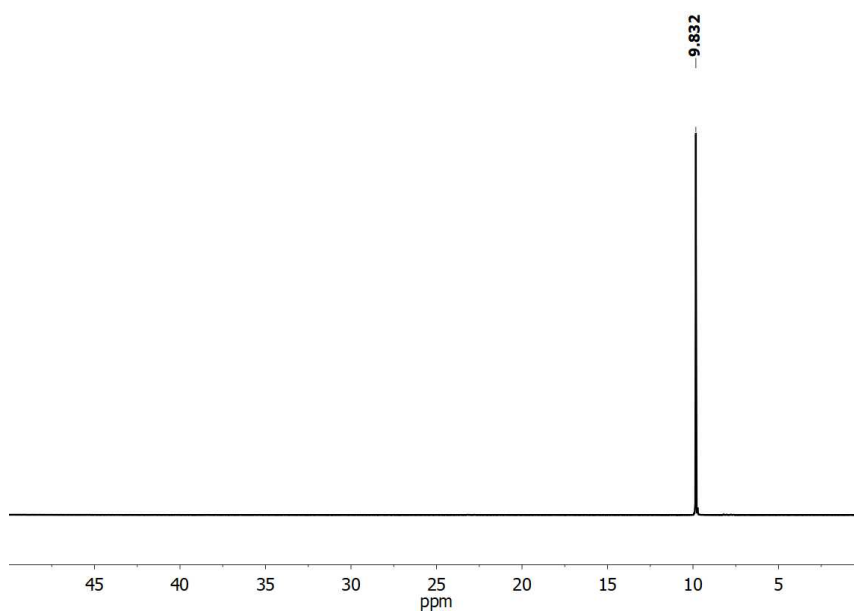


Figure S1. ^{31}P NMR spectrum of compound 5.

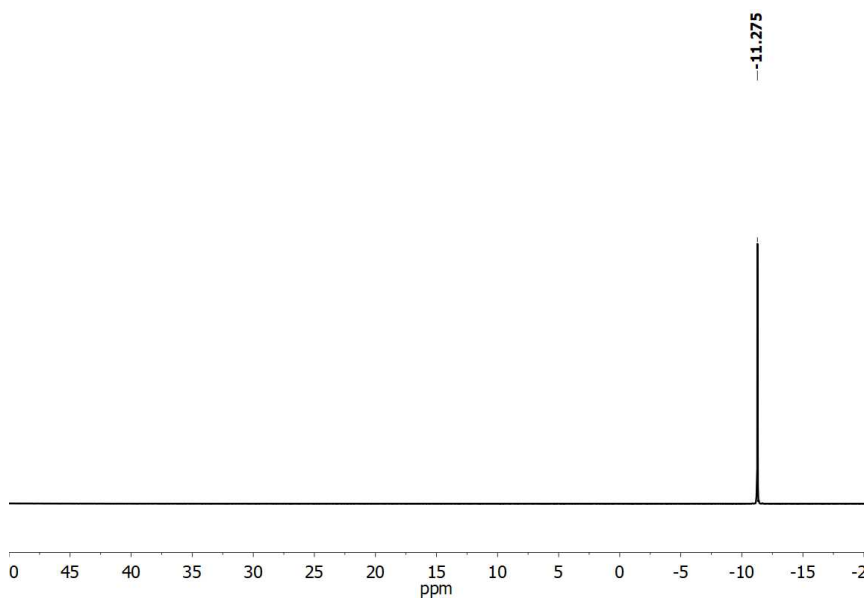


Figure S2. ^{31}P NMR spectrum of compound 7.

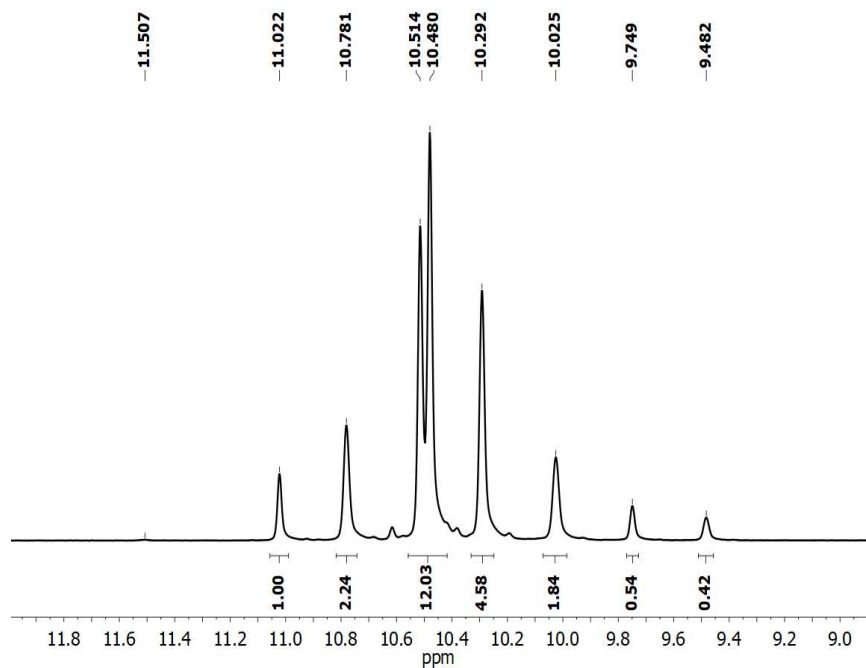


Figure S3. ^{31}P NMR spectrum of compound **6**.

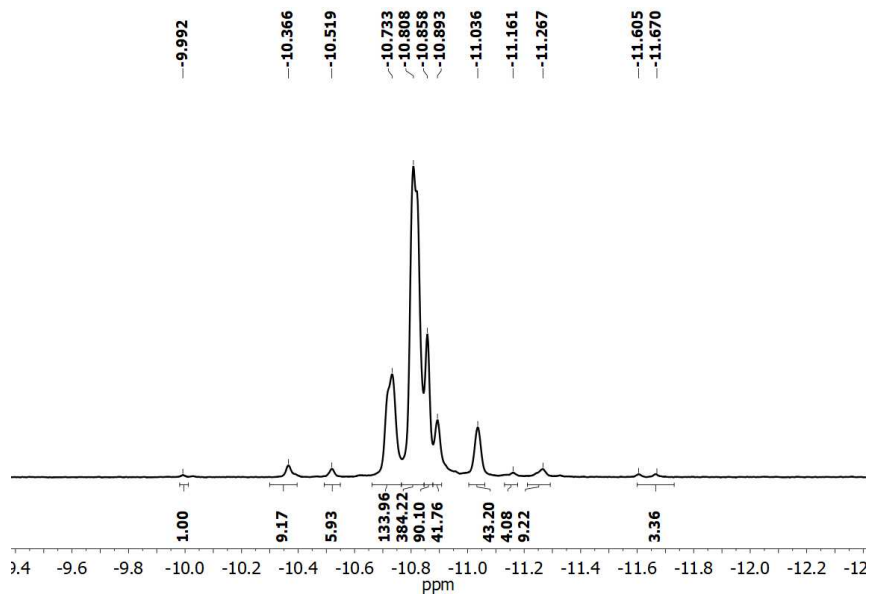


Figure S4. ^{31}P NMR spectrum of compound **8**.

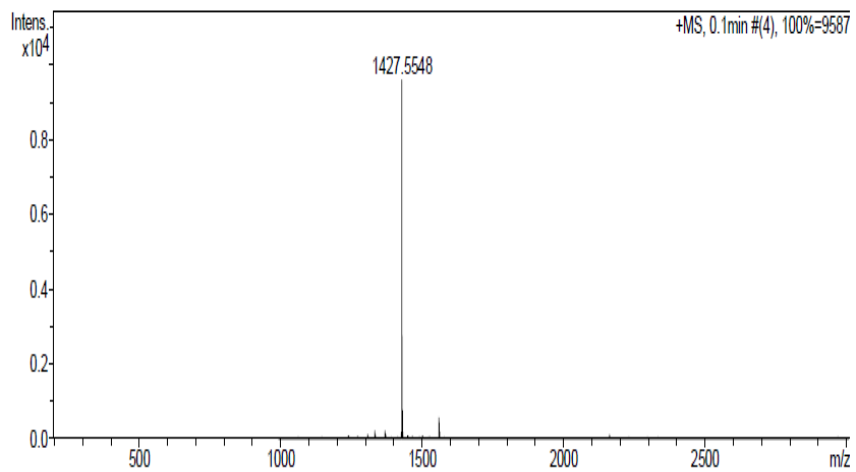


Figure S5. Mass spectrum of compound 5.

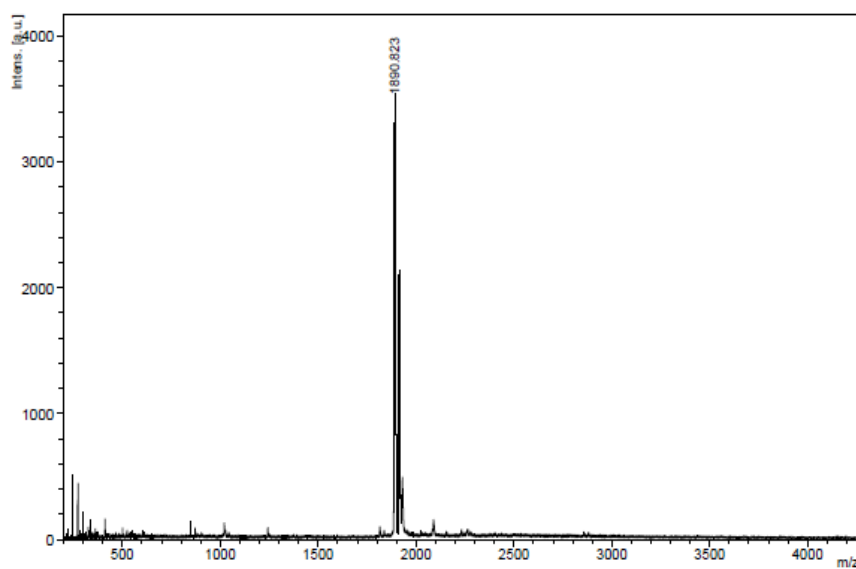


Figure S6. Mass spectrum of compound 7.

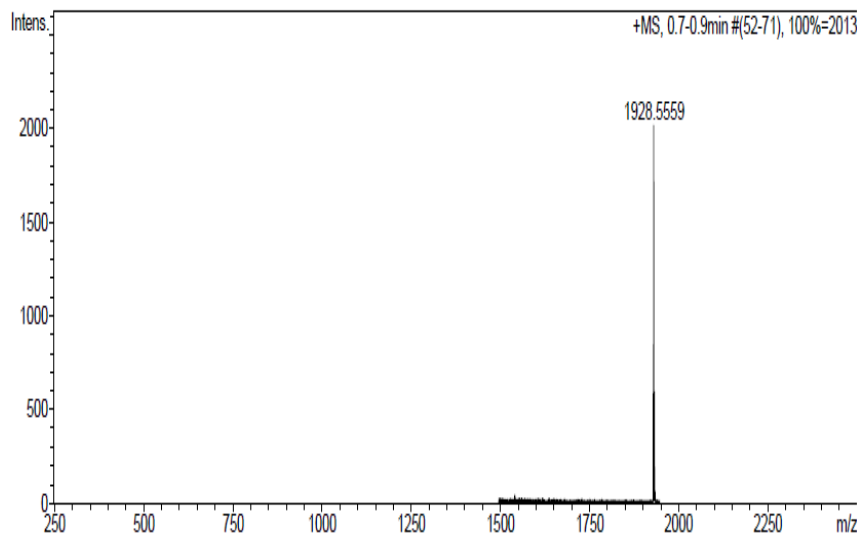


Figure S7. Mass spectrum of compound 6.

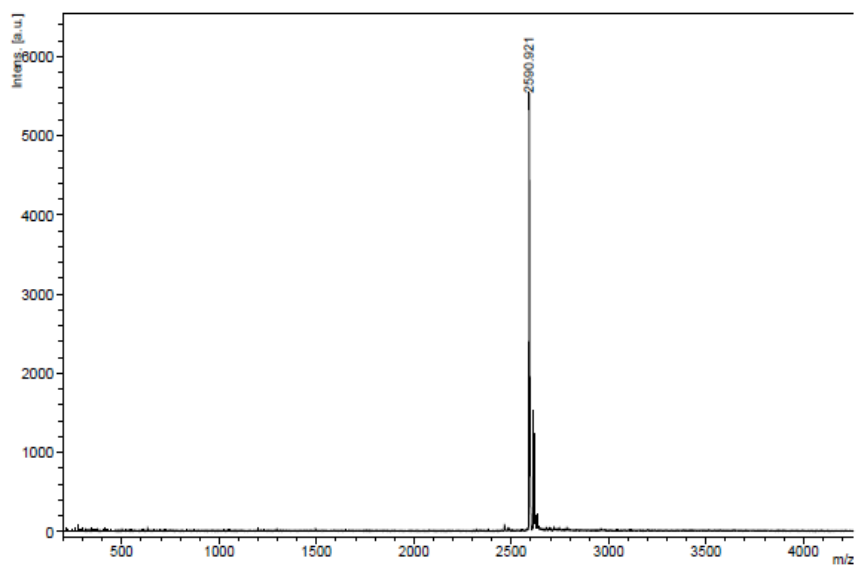


Figure S8. Mass spectrum of compound 8.

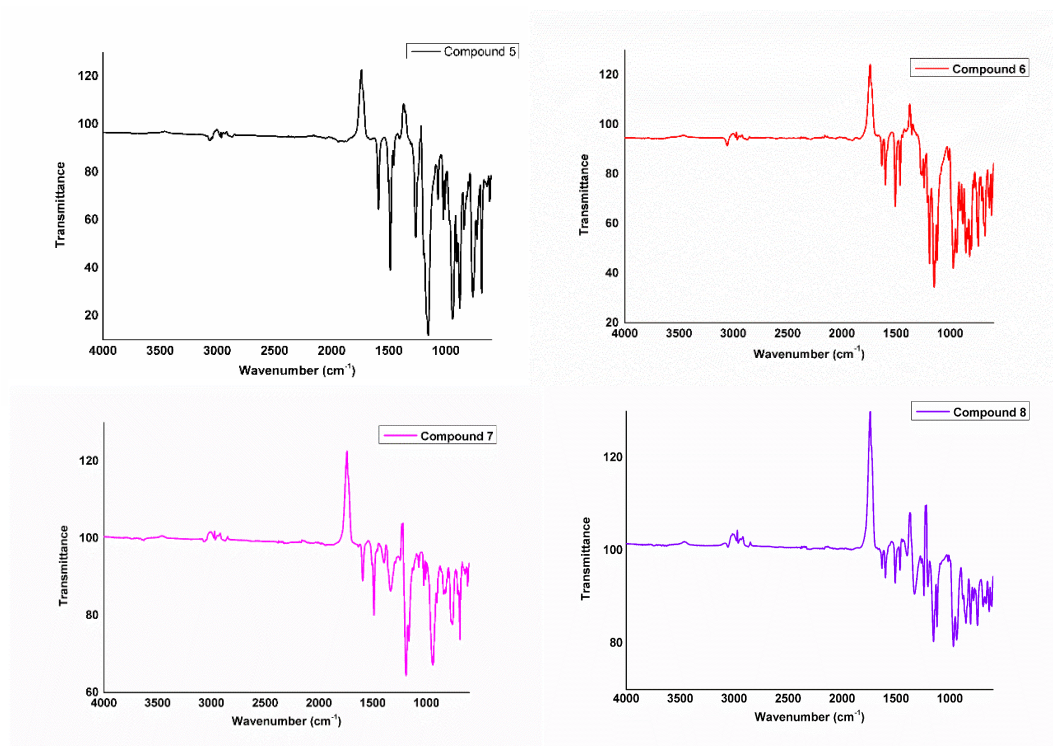


Figure S9. FTIR spectrum of compounds **5**, **6**, **7**, and **8**.

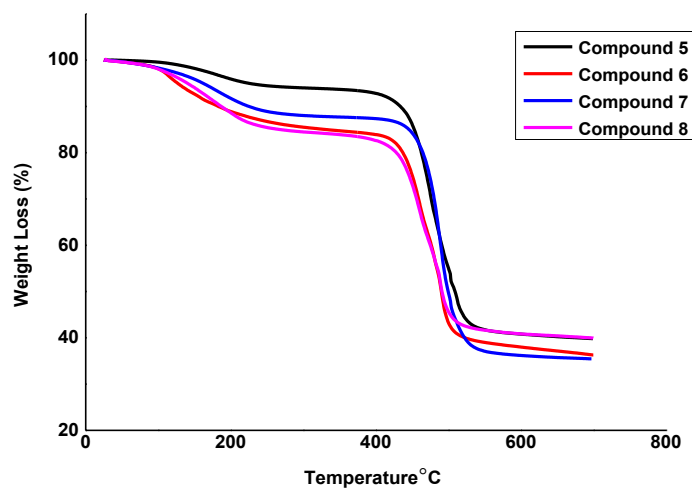


Figure S10. TGA thermograms of compounds **5**, **6**, **7**, and **8**.

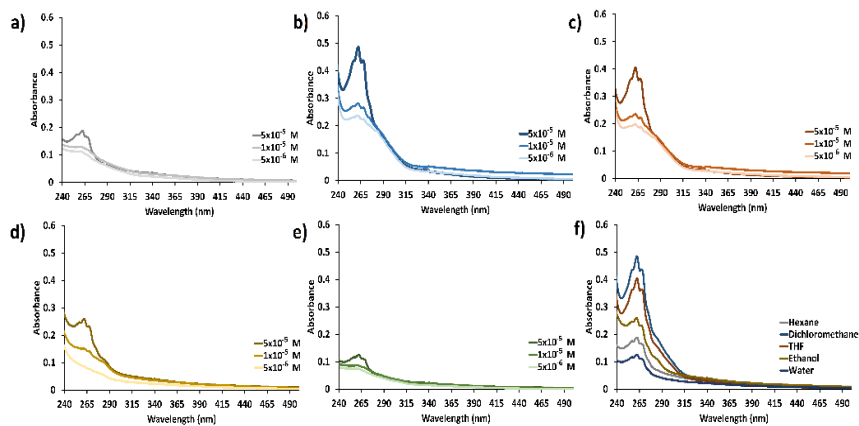


Figure S11. UV-Vis absorption spectra of compound **5** in (a) hexane, (b) DCM, (c) THF, (d) ethanol, and (e) water at various concentrations, and (f) overlap spectra of the solvents at 5×10^{-5} M.

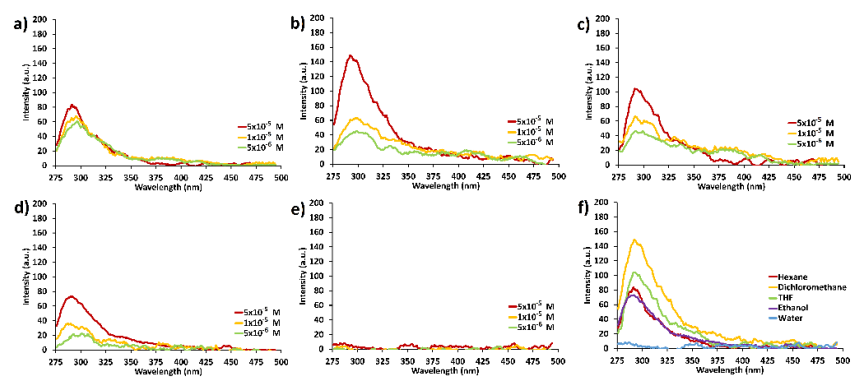


Figure S12. Fluorescence emission spectra of compound **5** in (a) hexane, (b) DCM, (c) THF, (d) ethanol, and (e) water at various concentrations, and (f) overlap spectra of the solvents at 5×10^{-5} M ($\lambda_{exc.}$: 260 nm).

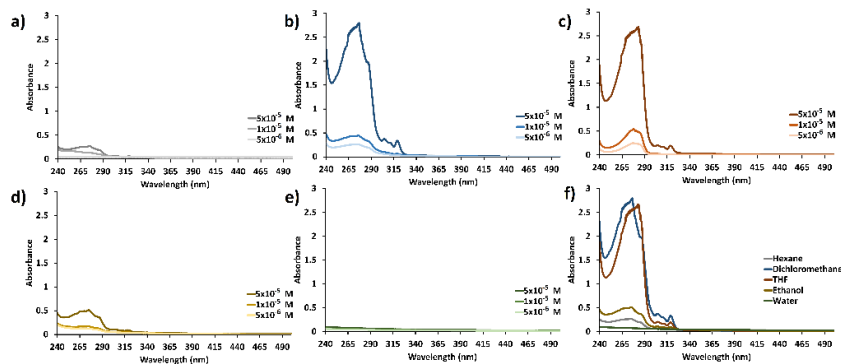


Figure S13. UV-Vis absorption spectra of compound **6** in (a) hexane, (b) DCM, (c) THF, (d) ethanol, and (e) water at various concentrations, and (f) overlap spectra of the solvents at 5×10^{-5} M.

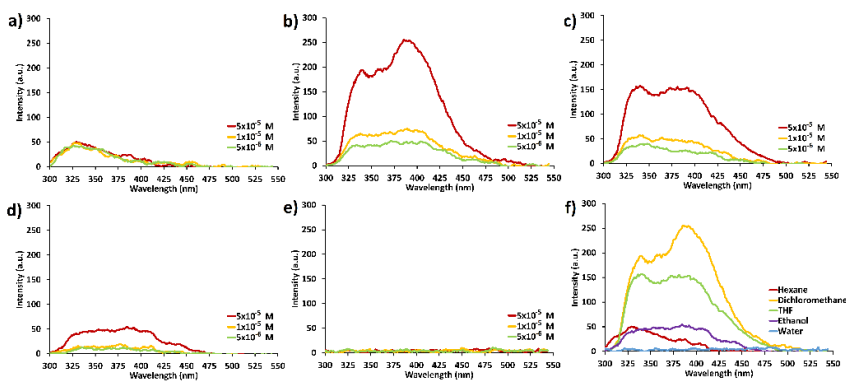


Figure S14. Fluorescence emission spectra of compound **6** in (a) hexane, (b) DCM, (c) THF, (d) ethanol, and (e) water at various concentrations, and (f) overlap spectra of the solvents at 5×10^{-5} M ($\lambda_{exc.}$: 290 nm).

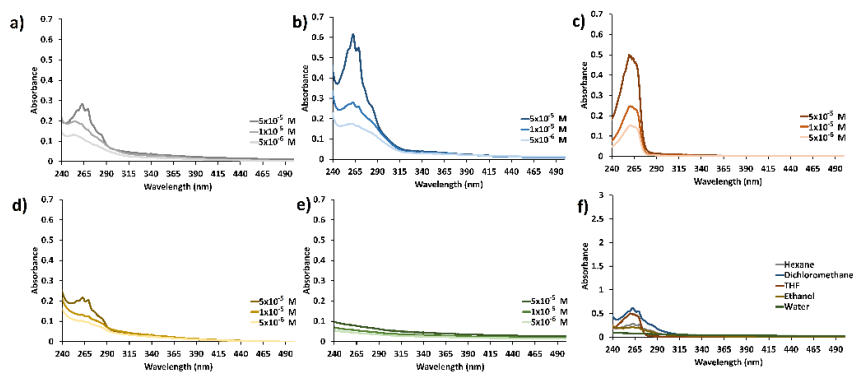


Figure S15. UV-Vis absorption spectra of compound **7** in (a) hexane, (b) DCM, (c) THF, (d) ethanol, and (e) water at various concentrations, and (f) overlap spectra of the solvents at 5×10^{-5} M.

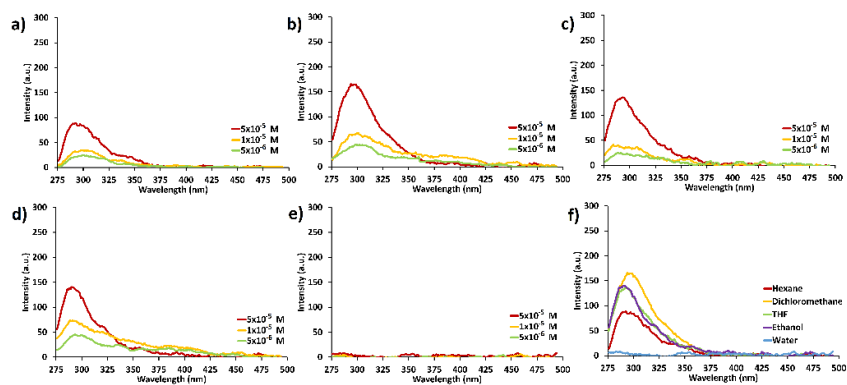


Figure S16. Fluorescence emission spectra of compound **7** in (a) hexane, (b) DCM, (c) THF, (d) ethanol, and (e) water at various concentrations, and (f) overlap spectra of the solvents at 5×10^{-5} M ($\lambda_{exc.}$: 260 nm).

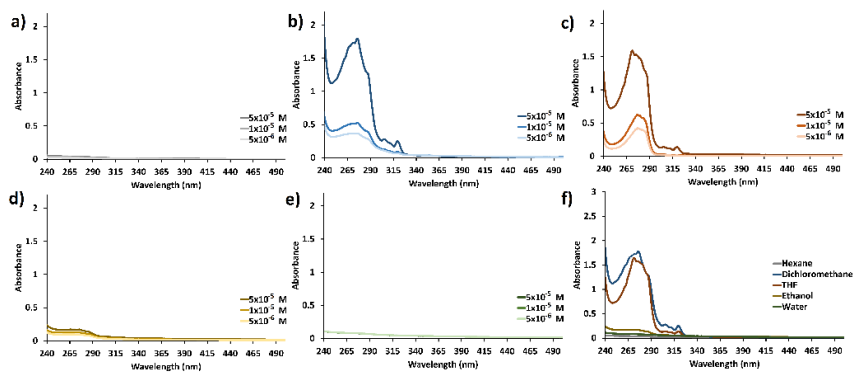


Figure S17. UV-Vis absorption spectra of compound **8** in (a) hexane, (b) DCM, (c) THF, (d) ethanol, and (e) water at various concentrations, and (f) overlap spectra of the solvents at 5×10^{-5} M.

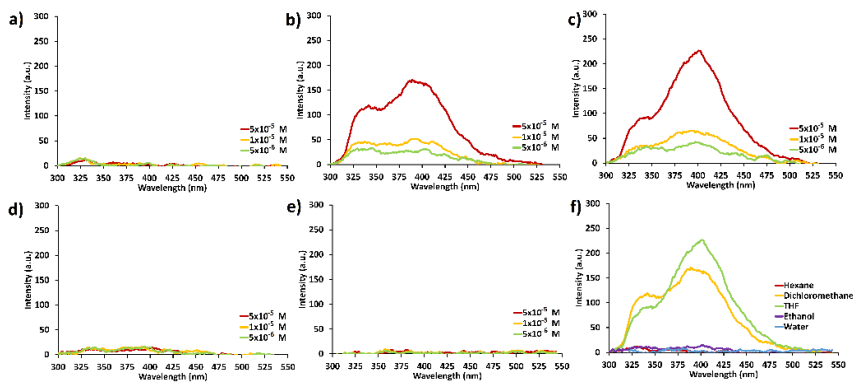


Figure S18. Fluorescence emission spectra of compound **8** in (a) hexane, (b) DCM, (c) THF, (d) ethanol, and (e) water at various concentrations, and (f) overlap spectra of the solvents at 5×10^{-5} M ($\lambda_{exc.}$: 290 nm).